

# Computational analysis of folding and mutation properties of C5 domain from Myosin binding protein C

Carlo Guardiani

*Centro Interdipartimentale per lo Studio delle Dinamiche Complesse (CSDC)  
Sezione INFN di Firenze, (Italy)*

Fabio Cecconi

*INFM-SMC and Istituto dei Sistemi Complessi ISC-CNR,  
Rome Italy*

Roberto Livi

*Dipartimento di Fisica Università di Firenze  
Centro Interdipartimentale per lo Studio delle Dinamiche Complesse (CSDC),  
Sezione INFN di Firenze e INFM UdR Firenze, Italy.*

Thermal folding Molecular Dynamics simulations of the domain C5 from Myosin Binding Protein C were performed using a native-centric model to study the role of three mutations related to Familial Hypertrophic Cardiomyopathy. Mutation of Asn755 causes the largest shift of the folding temperature, and the residue is located in the CFGA'  $\beta$ -sheet featuring the highest  $\Phi$ -values. The mutation thus appears to reduce the thermodynamic stability in agreement with experimental data. The mutations on Arg654 and Arg668, conversely, cause a little change in the folding temperature and they reside in the low  $\Phi$ -value BDE  $\beta$ -sheet, so that their pathologic role cannot be related to impairment of the folding process but possibly to the binding with target molecules. As the typical signature of Domain C5 is the presence of a longer and destabilizing CD-loop with respect to the other Ig-like domains we completed the work with a bioinformatic analysis of this loop showing a high density of negative charge and low hydrophobicity. This indicates the CD-loop as a *natively unfolded sequence* with a likely coupling between folding and ligand binding.

**Keywords:** Simulations, Myosin binding protein C, Folding, Mutations, Natively Unfolded Proteins;

## I. INTRODUCTION

Familial Hypertrophic Cardiomyopathy (FHC) is a genetic disease causing significant impairment of cardiac functionality and premature death in children and young adults [1]. A number of mutations in genes encoding cardiac sarcomeric proteins including the  $\beta$ -myosin heavy chain, the cardiac troponin T, titin, and cardiac myosin binding protein C (MyBP-C) have been found to correlate with such disease [2, 3, 4, 5, 6]. The FHC patients with MyBP-C mutations represent 20-45 % of the total [7, 8], so that mutations on this protein are the second most common cause of the disease. While nonsense mutations on MyBP-C gene determine a premature termination of translation of the C-terminus and result in a mild phenotype [7, 8, 9], a number of missense mutations lead to a severe phenotype and the precise mechanism through which they cause the disease is still unknown [10, 11]. MyBP-C is a linear sequence of 11 IgI-like and fibronectin-like domains referred to as C0-C10 working as a potential regulator of cardiac contractility [1]. According to Moolman-Smook model [12, 13], three MyBP-C molecules form a ring around the thick filaments (Figure 1). The collar is stabilized by specific interactions between domains C5-C8 of a molecule and domains C7-C10 of the neighboring one. The amino-

terminal region between domains C0 and C4 protrudes out of the thick filament and, upon phosphorylation, interacts with subfragment 2 of Myosin (S2) acting as a brake for muscular contraction [14]. Mutations on MyBP-C might either prevent the C0-C4 region from interacting with the S2 fragment (hyper-contractility) or force a carboxy-truncated mutant to permanently interact with S2 (hypo-contractility) [13, 15].

Our work will be concerned with the folding behavior of domain C5 whose structure was resolved through NMR by Idowu et al. [16]. This domain belongs to the IgI set of the Immunoglobulin superfamily and it features a typical  $\beta$ -sandwich structure with two twisted  $\beta$ -sheets closely packed against each other. The first  $\beta$ -sheet ( $\beta_1$ ) is formed by strands C,F,G and A', while the second  $\beta$ -sheet comprises strands B,D and E (see Fig. 5). A remarkable peculiarity of the C5 domain of the cardiac MyBP-C isoform is the presence of two long insertions not present in the fast and slow skeletal isoforms. The first insertion is 10-residue long and is located in the linker between the C4 and C5 domains; the second insertion is 28 residues in length and resides in the CD loop [16].

A recent experimental work [16] proved that the N-terminal region containing the first insertion is not just a linker between C4 and C5, but it plays an important role in the thermodynamical stability of the domain. Conversely, the long and highly mobile prolin-reach CD-loop destabilizes the protein lowering the folding temperature as compared to other Ig-domains[16]. This loop is

suspected to form an SH3 domain recognition sequence presumably binding to the CaM-II like Kinase that copurifies with MyBP-C [17, 18].

Three FHC causing mutations have been identified on C5 domain: Asn755Lys, Arg654His and Arg668His. The first one lies on the FG-loop and leads to a significant destabilization of the protein yielding a severe phenotype [12, 16, 19]. The Arg654His and Arg668His mutations, related to a much milder phenotype, are reported not to impair the thermodynamic stability of the protein. Residue Arg654 is actually suspected to regulate the specificity of the binding of positively charged substrates, as it is located in the negatively charged CFGA' face that is a potential target for the binding with domain C8 [10, 12, 16]. A role in ligand binding is also postulated for Arg668 [20].

The purpose of the present work is to investigate through MD simulations the role of the above mentioned three known FHC causing mutations. Clarke and coworkers showed that for the proteins belonging to the Ig-superfamily both transition and native states are stabilized by the same contacts dictated by protein topology [21]. This implies that the Ig-superfamily members share similar folding pathways mainly determined by their common geometry. Therefore the native-centric approach seems to be the natural framework to investigate the folding properties of Ig-like C5 domain. To incorporate topology and some specific chemical feature as well as the effect of the side chain packing we resorted to consider a heavy-map Gō model where native contacts are identified on the basis of the steric hindrance of side-chains. Moreover we also introduced some amount of heterogeneity in the energetic couplings of the Gō force field. This approach is particularly suitable for the C5 domain because we need to address the problem of discriminating the effects of mutations such as Arg654His and Arg668His modeled through the removal of the same number of native contacts.

The importance of introducing energetic heterogeneity in a Gō-model for a reliable mutation analysis, is showed for example, by the work of Clementi *et al.* [22], where all the available experimental data on free energy differences upon single mutations of S6 ribosomal protein and its circular permutants, were reproduced with correlation coefficients larger than 0.9.

## II. METHODS

When the folding process is mainly driven by the topological constraints of the native state, it is convenient to use simplified coarse-grained models describing the protein molecule as a chain of beads centered on the  $C_\alpha$  carbon positions [23, 24, 25, 26, 27, 28]. The Gō force field introduces a bias towards native structure rewarding native-like interactions, through Lennard-Jones attractive forces and appropriate angular potentials embodying secondary structure motifs. The approach assigns to the

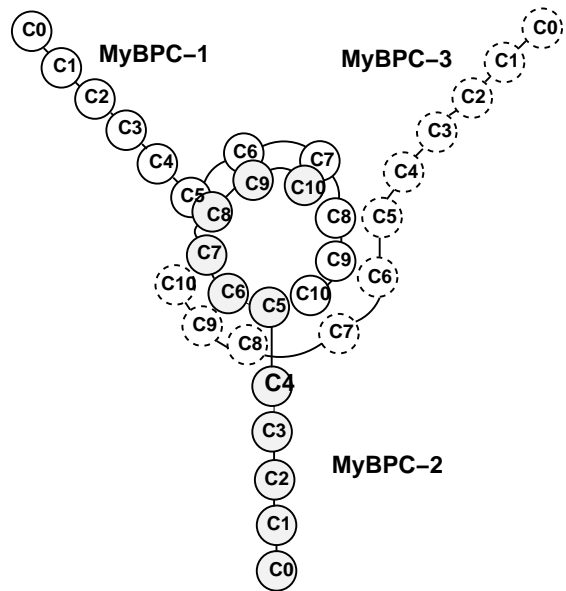


FIG. 1: Moolman-Smook model of MyBP-C arrangement in the sarcomere: the trimeric collar surrounding the thick filament is stabilized by interactions between domains C5-C8 and C7-C10.

native state the lowest energy and minimizes frustration yielding a perfect funnel landscape. We consider a light variant of the Gō-like force field proposed by Clementi *et al.* and used in several other papers [29, 30, 31]. The model is defined by the Potential Energy [32]:

$$V_{tot} = \sum_{i=1}^{N-1} \frac{k_h}{2} (r_{i,i+1} - R_{i,i+1})^2 + \sum_{i=2}^{N-1} \frac{1}{2} k_\theta (\theta_i - \theta_i^0)^2 + \sum_{i=3}^{N-2} k_\phi^{(1)} [1 - \cos(\phi_i - \phi_i^0)] + k_\phi^{(3)} [1 - \cos 3(\phi_i - \phi_i^0)] + \sum_{i,j>i+3} V_{nb}(r_{ij}) \quad (1)$$

Where the last potential corresponding to non bonded interaction is such that

$$V_{nb}(r_{ij}) = \begin{cases} \epsilon_{ij} \left[ 5 \left( \frac{R_{ij}}{r_{ij}} \right)^{12} - 6 \left( \frac{R_{ij}}{r_{ij}} \right)^{10} \right] & i - j \text{ native} \\ 5\epsilon_r \left( \frac{\sigma}{r_{ij}} \right)^{12} & i - j \text{ not native} \end{cases} \quad (2)$$

In the above formulas,  $r_{ij}$  is the distance between residue  $i$  and  $j$ ,  $\theta_i$  is the bending angle identified by the three consecutive  $C_\alpha$ 's  $i-1, i, i+1$ ,  $\phi_i$  is the dihedral angle defined by the two planes formed by four consecutive  $C_\alpha$ 's  $i-2, i-1, i, i+1$ . The symbols with the superscript 0 and  $R_{ij}$  are the corresponding quantities in the native conformation. The force field parameters are proportional to the energy scale  $\epsilon_0 = 0.3$  Kcal/mol such that  $k_h = 1000\epsilon_0/r_0^2$  ( $r_0 = 3.8$  Å),  $k_\theta = 20\epsilon_0$ ,  $k_\phi^{(1)} = \epsilon_0$  and  $k_\phi^{(3)} = 0.5\epsilon_0$ . The parameters of the repulsive Lennard-Jones terms between

non native contacts are chosen as follows:  $\sigma = 5.0 \text{ \AA}$ ,  $\epsilon_r = 2/3\epsilon_0$ . Two residues  $i$  and  $j$  are considered to interact attractively whenever their side-chains have at least a pair of heavy atoms closer than a distance cutoff  $R_c = 5 \text{ \AA}$ . Accordingly, the attractive native interactions depend on the coefficients  $\epsilon_{ij} = \epsilon_0(1 + n_{ij}/n_{max})$ , where  $n_{ij}$  is the number of atomic contacts between residues  $i$  and  $j$  in their native position and  $n_{max} = 43$  is the maximum value of  $n_{ij}$  in the set of native contacts corresponding to the couple Lys45-Tyr109. We performed controlled temperature MD simulations employing the isokinetic thermostat [33] with time step  $h = 5 \times 10^{-3}\tau$ , where the time unit  $\tau = \sigma\sqrt{M/\epsilon_0} = 4.67 \text{ ps}$  ( $M$  is the average mass of an aminoacid residue estimated to 110 Da).

As a remark we observe that several strategies can be employed to introduce heterogeneity. A very common choice is to use the set of parameters derived by Miyazawa and Jernigan [34, 35]. Other authors [32] instead prefer to tune the energy parameters through a design procedure based on energy gap maximization. Our strategy of rescaling the contact energies according to the number of atomic contacts is grounded on experimental and theoretical evidence. In particular, the mutation analysis on barnase by Serrano *et al.* [36] showed a non trivial correlation between the destabilization induced by the mutation and the number of methyl or methylene side groups surrounding the deleted group. Moreover, Kurochkina and Lee [37], found that the pairwise sum of the buried surface area is linearly related to the true buried area, as computed with the algorithm of Lee and Richards [38] and to the contact potential of Miyazawa and Jernigan [34]. The approach proposed by Kurochkina was then followed by Sung [39] for an efficient modeling of the hydrophobic effect in a Monte Carlo study of  $\beta$ -hairpin folding. A significant correlation between the average contribution of individual residues to folding stability and the buried ASA was also noticed by Zhou and Zhou [40]. To check that heterogeneity we have introduces does not lead to excessive frustration in the energy landscape, we performed rapid quenching simulations to collect a data set  $10^3$  of decoys. We then estimate the ratio  $T_g/T_f$  between the glassy and folding temperature of our protein as the ratio: energetic standard deviation of the decoy set over the energy gap. We found that this quantity which is a measure of the energy landscape frustration remained substantially unaltered from the heterogeneous G $\bar{o}$ -model,  $T_g/T_f = 0.34$ , to the homogeneous one  $T_g/T_f = 0.35$ .

A customary indicator of the native-likeness of residues in the transition state (TS) is represented by the  $\Phi$ -values: a value  $\Phi \sim 1$ , characterizes residues establishing native-like interactions already in the TS, whereas a value close to zero is typical of residues involved into a disordered conformation in the TS. We apply the free energy perturbation technique (FEP) [32] to evaluate the

$\Phi$ -values from our MD simulations

$$\Phi = \frac{\log\langle\exp\{-\Delta E/RT\}\rangle_{TS} - \log\langle\exp\{-\Delta E/RT\}\rangle_U}{\log\langle\exp\{-\Delta E/RT\}\rangle_F - \log\langle\exp\{-\Delta E/RT\}\rangle_U} \quad (3)$$

where the Boltzmann factors depend on the energy difference between the mutant and the wild type (WT) and the averages are computed over WT-conformations of the folded (F), transition state (TS) and unfolded (U) ensembles. In the present paper, the  $\Phi$ -values are computed according to equation 3 using a method developed by Clementi *et al.* [32] that can be summarized in the following steps. i) Determination of the folding temperature  $T_f$  from the specific heat plot. ii) Analysis of the free energy profile at temperature  $T_f$  plotted as a function of a suitable folding reaction coordinate. The double-well free energy profile of a two-state folder allows to define three windows of the reaction coordinate identifying the folded, transition state and unfolded ensembles respectively. iii) Dynamic simulation at  $T = T_f$  and storage of conformations belonging to the F, TS and U ensembles. vi) Choice of mutations and computation of FEP  $\Phi$ -values (3).

Structural information about the native-likeness of the transition state was also gained from the so-called structural  $\Phi$ -values:

$$\Phi_{struc}(i) = \frac{\sum_{j \in C(i)} P_{TS}(i, j)}{\sum_{j \in C(i)} P_F(i, j)} \quad (4)$$

where  $P_F(i, j)$  and  $P_{TS}(i, j)$  are the frequencies of the native contact  $i-j$  in the folded and transition ensembles respectively, and the sum runs over the set  $C(i)$  of native contacts in which residue  $i$  is involved.

An interesting property of the Transition State is the existence of a few *key residues* acting as nucleation centers for the folding process. Following an approach proposed by Vendruscolo *et al.* [41], the importance of these residues can be better understood by portraying the protein as a weighted graph. Residues represent the vertices and the weighted edges are defined as  $w_{ij} = 1/A_{ij}$  where  $A_{ij}$  represents the fraction of TS ensemble structures where residues  $i$  and  $j$  are in contact. By using the Dijkstra's algorithm [42] we computed the minimal path  $\lambda_{ij}$  *i.e.* the minimum of the sum of the weights  $w_{kl}$  of the edges traversed along each route between  $i$  and  $j$ . The fraction of minimal paths passing through residue  $k$  defines the *betweenness*  $B_k$  of that residue. This quantity therefore measures the centrality of a residue: residues with a high betweenness act as "hubs" in the network and they presumably play a crucial role in the stabilization of the transition state.

### III. RESULTS

A thermal folding simulation of the wild-type (WT) C5-domain was performed by gradually cooling the protein from temperature  $T = 2.5$  to  $T = 1.5$  in 50 temperature steps. For each temperature, an equilibration stage

Species	$T_{exp}[K]$	$T_{sim}[K]$	$\kappa_2$
WT	$322.06 \pm 0.75$	$322 \pm 3$	0.976
Mut14	$318.46 \pm 1.44$	$322 \pm 3$	1.0
Mut28	N.A.	$317 \pm 3$	0.989
Mut115	$309.36 \pm 0.41$	$313 \pm 3$	1.0
$\Delta$ 1-7	N. A.	$311 \pm 4$	1.0

TABLE I: Experimental and simulated folding temperatures of WT domain C5 of MyBP-C and its mutants. The last column reports the cooperativity parameters  $\kappa_2$ . N.A. = Not Available Data.

of  $5 \times 10^7$  time steps was followed by a production stage of  $5 \times 10^8$  time steps. A similar schedule was employed to simulate the folding of the three missense mutants Asn115Lys, Arg14His and Arg28His (notice that protein residues have been renumbered 1-130 as a restriction to the C5 domain only). Within the framework of the G $\bar{o}$ -model, we decided to implement a mutation of a residue by turning all its native contacts into non-native ones. The role of the amino-terminal region of the protein was also investigated through folding simulations of a deletion mutant, where the first 7 residues of the C5 domain were removed.

The specific heat profiles, displayed in Figure 2, show that the WT C5-domain and the missense mutants fold according to a cooperative, two-state mechanism as quantified by the van't Hoff criterion [43] determined by parameter  $\kappa_2 = 2T_f \sqrt{k_B C_v(T_f)} / \Delta H_{cal}$  expressing the ratio between the van't Hoff and the calorimetric enthalpies after appropriate baseline subtraction [44] in energy or  $C_v$  plots. A value of  $\kappa_2$  close to unity indicates a very cooperative behavior of the folding transition. Table III summarizes the  $\kappa_2$  values along with the experimental and theoretical transition temperatures.

Figure 2 also shows that a mutation on Arg14 hardly has any effect on the thermodynamic stability of the protein as the thermogram of this mutant is almost perfectly superposed to that of the wild-type. A mutation on Arg28, conversely, determines a shift of the folding temperature to lower values and the shift in  $T_f$  is even larger for a mutation on Asn115. It is worthwhile noticing that the different stability of Mut14 and Mut28 is appreciated only using the heterogeneous model while the peaks of the two  $C_v$  plots remain unsolved for the homogeneous G $\bar{o}$ -model. Apart for this difference in the resolution power, however the relative positions of the  $T_f$  remains unchanged in the two models. The destabilizing effect of the mutation on Asn115 appearing from our simulations is in agreement with CD and NMR spectra recorded by Idowu *et al.* [16] showing that the Asn115Lys mutant is unstable and largely unfolded as compared to the wild-type C5 motif. The same authors [16] also noticed that the Arg14His mutant is as well folded and as stable as the wild-type which, again, is consistent with the good superposition of the thermograms of the wild-

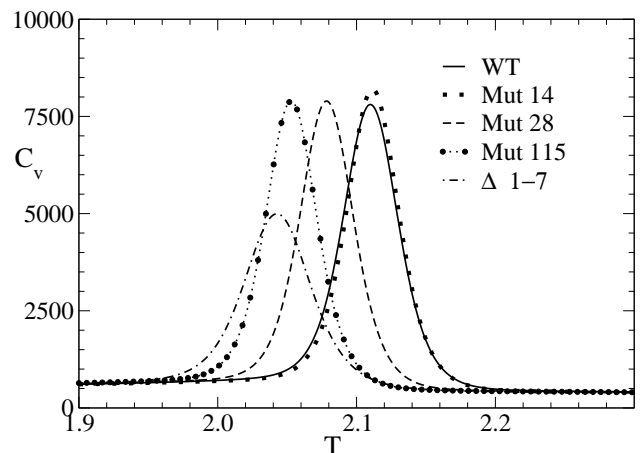


FIG. 2: Thermal behavior of heat capacity of the WT C5 domain, the missense mutants deprived of the native contacts of Arg14, Arg28 and Asn115, and the deletion mutant lacking the 1-7 subsequence. Computations have been performed processing with the weighted histogram method the data collected during folding simulations. The temperature is measured in units  $\epsilon_0/R = 151.1$  K and  $C_v$  in units  $R = 1.9855 \times 10^{-3}$  Kcal mol $^{-1}$ K $^{-1}$ .

type and Arg14 mutants found in our simulations. However, it is important to notice that, while the Asn115Lys mutant appears to be largely unfolded in mutagenesis experiments, a folding simulation using the G $\bar{o}$ -model always ends up in the correct native structure and the only trace of a mutation is a shift in  $T_f$ . This is due to the fact that the G $\bar{o}$ -model introduces a bias towards the native state so strong to override the disruptive effect of most mutations.

The 1-7 deletion mutant finally appears to be the most destabilized one as it produces the largest shift in  $T_f$ . This result is also consistent with the observation by Idowu and coworkers that the  $\Delta 1 - 7$  mutant remains largely unfolded. The effect of the three FHC-related mutations was further investigated through  $\Phi$ -value analysis. The free energy profile of the WT protein as a function of the overlap  $Q$  (fraction of native contacts) at the folding temperature  $T_f = 2.1$ , shows the typical double-well pattern of two-state folders as illustrated in Figure 3.

The well centered values on low overlap correspond to the unfolded state ensemble (U), whereas the well insisting in the high overlap region is related to the folded state ensemble (F). The barrier between the two wells represents the transition state ensemble (TS). Conformations belonging to the F, TS and U ensembles can thus be sampled by the choice of three appropriate windows of the reaction coordinate  $Q$  (Fig. 4), and used for the computation of  $\Phi$ -values using the perturbation approach (Methods).

The domain C5 results to be asymmetric with respect to the distribution of FEP  $\Phi$ -values, in particular the

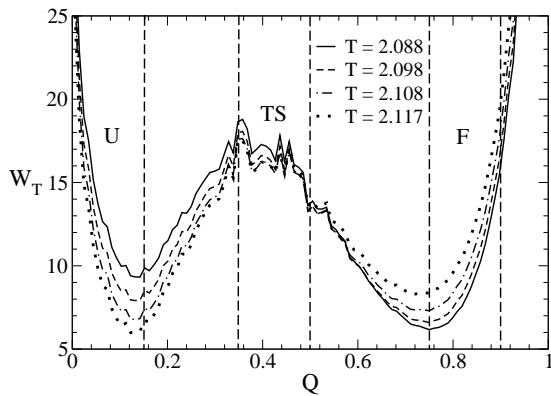


FIG. 3: Profiles of potential of mean force versus overlap around the folding temperature  $T_f = 2.1$ . The Figure shows three windows of overlap corresponding to the Unfolded ( $0 < Q < 0.15$ ), Transition State ( $0.35 < Q < 0.5$ ) and Folded State Ensemble ( $0.75 < Q < 0.9$ ).

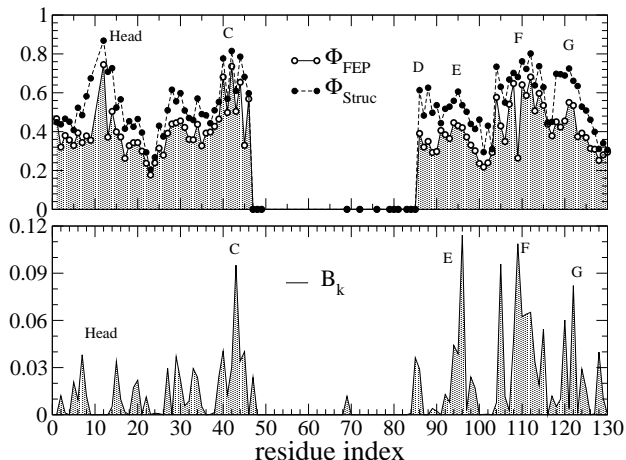


FIG. 4: Structural and perturbation  $\Phi$ -values (top panel) compared to the betweenness (bottom panel): the similarity between the profiles of  $\Phi$ -values and betweenness suggests that the key residues stabilizing the TS, derive their importance from their centrality in the network of contacts of the protein. The three profiles were computed using the conformations sampled in a run at folding temperature  $T_f = 2.1$  in the three windows of overlap shown in Fig. 3. "Head" refers to the N-terminal 1-17 region.

sheet containing the longest strands ( $\beta_1$ ) is characterized by high  $\Phi$ -values while the sheet formed by the shorter strands ( $\beta_2$ ) has low  $\Phi$  values (Figure 5). This result is in agreement with what suggested by Clarke and coworkers [21]. In fact, the long-stranded sheet  $\beta_1$ , derives its high stability from the presence of many contacts chemically corresponding to hydrogen bonds. The contacts more contributing to the stability, however, are the same that stabilize the TS. Thus the sheet more important for the stability ( $\beta_1$ ) is also the sheet whose formation represents the rate limiting step in the folding kinetics. A more

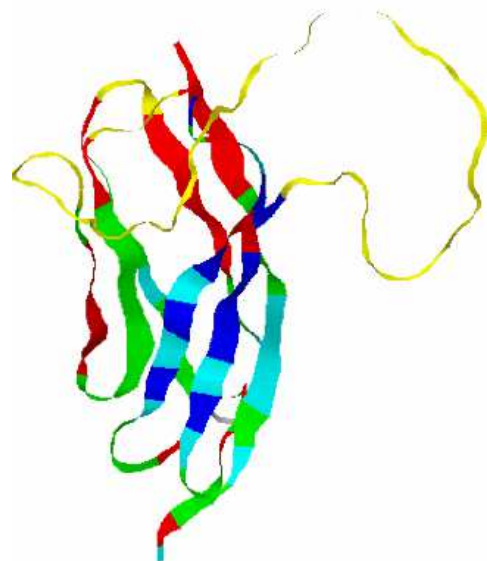


FIG. 5: Color-coded distribution of perturbation  $\Phi$ -values on the structure of the C5 domain. Yellow:  $\Phi < 0.25$ ; Red:  $0.25 < \Phi < 0.35$ ; Green:  $0.35 < \Phi < 0.45$ ; Cyan:  $0.45 < \Phi < 0.55$ ; Blue:  $0.55 < \Phi < 0.75$ . The blue and cyan regions corresponding to the highest  $\Phi$ -values are concentrated on strands C, F and G. The BDE sheet conversely is characterized by low  $\Phi$ -values.

detailed picture of the transition state is provided by Figure 6 displaying a contact map where contact  $\Phi$ -values are quantified by a color scale. The most important contacts stabilizing the TS are those between strands C and F and strands F and G. A minor contribution to the stability of the TS is also provided by the contacts linking the central parts of strands B and A' and Head-Head contacts (where "Head" corresponds to the N-terminal 1-17 segment). Structural  $\Phi$ -values offer supplementary data complementing the scenario supplied by the FEP analysis. The two indicators in fact store different information: high FEP  $\Phi$ -values identify those residues whose mutation most destabilizes the TS. Whereas high structural  $\Phi$ -values characterize residues in a native-like conformation in the TS regardless of whether they actively stabilize the structure or they were passively driven in a correct native-like conformation by the rearrangement of neighboring regions of the molecule. This pattern was also observed in an experimental study on a fibronectin-like domain reported in Ref. [45]. The peculiar features of the two indicators thus explain why structural  $\Phi$ -values are systematically higher than FEP  $\Phi$ -values. The difference between structural and perturbation  $\Phi$ -values yields a profile whose peaks identify the residues passively driven in a native-like conformation in the TS: this residues are mainly located on strand D and at the boundary between strands F and G. It can also be noticed that Pro12 plays an active role in stabilizing the N-terminal region in a native-like conformation in the TS, while His8 and

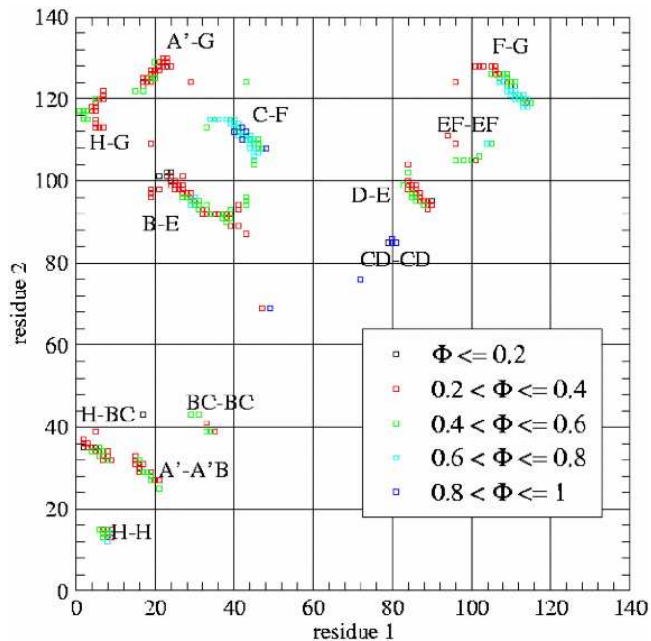


FIG. 6: Bond  $\Phi$ -values. The color-coded contact map shows that the C-F and F-G contacts feature the highest  $\Phi$ -values and they thus provide the most relevant contribution to the stability of the TS. The symbol "H" designates the amino-terminal 1-17 segment.

Gly13 are just passively placed in the correct position.

The analysis of betweenness (Fig. 4) shows that this parameter, representing the fraction of minimal paths passing through a given residue, correlates well with the  $\Phi$ -values, in agreement with Ref. [41]. In particular, the betweenness confirms the importance of strands C, F and G but it differs from  $\Phi$ -values in two important regions of the protein. Strand E is characterized by a high betweenness as it is the central strand of the BDE sheet and it probably acts as a bridge between strands B and D: the importance of this strand may thus be higher than it appears from  $\Phi$ -values alone. Conversely, the N-terminal region of the protein is characterized by a low betweenness so that it appears to be weakly connected with the other parts of the molecule.

It is instructive to discuss the positions of the 3 FHC-related mutations within the two  $\beta$ -sheets of the C5 domain. In fact, Asn115 which lies on the sheet characterized by the highest FEP  $\Phi$ -values, when mutated to Lys, is known to completely disrupt the native structure of this protein. On the other hand, Arg14 and Arg28 are located on the sheet with low FEP  $\Phi$ -values and their mutation does not significantly affect the thermodynamic stability.

As a final remark, we tested the sensitivity of betweenness and structural and perturbative  $\Phi$ -values on the choice of the reaction coordinate. The computation protocol for these parameters has been repeated by using the Kabsch RMSD [46] as a collective coordinate for sampling

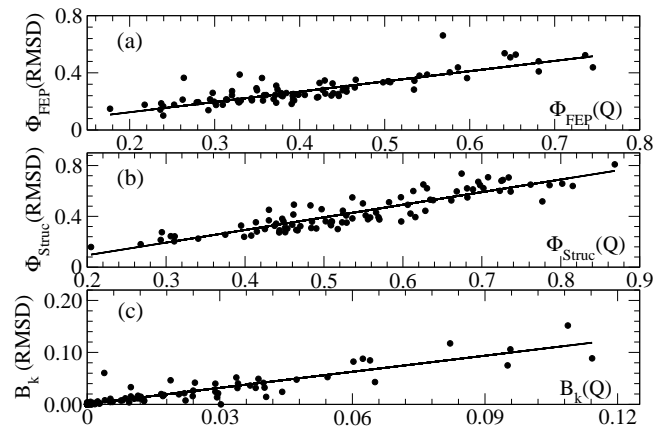


FIG. 7: Linear regression of parameters computed using the Kabsch RMSD and the fraction of native contacts  $Q$ . (a) Free energy Perturbative  $\Phi$ -values computed using Kabsch RMSD reaction coordinate versus the same quantity computed using the overlap  $Q$ . Correlation coefficient  $r = 0.8$ . (b) Structural  $\Phi$ -values (Kabsch RMSD) versus  $\Phi_{Struc}(Q)$ . Correlation coefficient  $r = 0.99$ . (c) Betweenness (Kabsch RMSD) versus  $B_k(Q)$ . Correlation coefficient  $r = 0.90$ .

of F, TS and U ensemble structures. The existence of linear relations (Fig. 7), with correlations coefficient greater than 0.8, between the parameters computed using either the Kabsch RMSD or the fraction of native contacts  $Q$  indicates that the sampling of the F, TS and U conformations is equivalent for the two methods. Thus the information conveyed by the parameters  $\Phi_{FEP}$ ,  $\Phi_{struct}$ ,  $B_k$  is statistically significant because not strongly dependent on the reaction coordinates used to compute them.

### A. The CD loop

As already mentioned in Section I, one of the most interesting features of the cardiac isoform of the C5 domain of MyBP-C is the presence of a 28 residue long insert that makes the CD loop significantly longer (residue 47 to 85) than the corresponding loop of the skeletal isoforms. Our simulations show that the CD loop is extremely mobile as it is involved in very few native contacts.

This high mobility of the CD loop is an extremely important feature of the C5 domain because it is responsible for a folding temperature significantly lower than that of most Ig domains [16]. The reasons for this unusual mobility can be clarified through a simple sequence analysis. First of all, we analyzed the hydrophobicity along the amino acid sequence using the Kyte and Doolittle scale [47]. The hydrophobicity of each residue was calculated by sliding a 5-residue long window over the protein sequence and assigning to the central residue the average hydrophobicity computed over the entire window. A similar approach was employed for the charge where Glu and Asp residues contribute -1, Lys and Arg contribute

+1 and the other residues are regarded as being neutral at physiological pH. The profiles in Figure 8 show that all the loops, and in particular the CD loop, feature an excess of negative charge and are less hydrophobic than the regions corresponding to the  $\beta$ -strands. An analysis

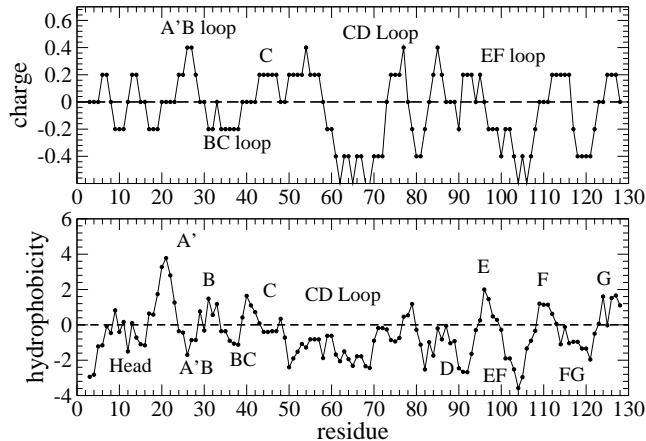


FIG. 8: Charge (top panel) and hydrophobicity (bottom panel) profiles along the protein sequence. Each value is an average over a 5-residue long window shifted along the polypeptide chain. Hydrophobicity was computed using the Kyte-Doolittle scale; regions with a positive value are hydrophobic. The CD loop appears to have a high density of negative charge and is scarcely hydrophobic. "Head" designates the 1-17 segment of the protein.

of the amino acid distribution along the chain, reveals a high concentration of charged residues in the CD loop where the number of Glu (4) and Asp (5) residues exceeds the number of Lys (3) and Arg (2) residues. A high concentration of Glu is also found in the EF loop. A remarkable feature is also the high concentration of Pro in the N-terminal 1-17 region, in the BC and in the CD loops. In summary, the CD loop is characterized by a high concentration of the residues identified by Garner *et al.* [48, 49, 50] as strong determinants of local disorder. Moreover, Uversky [51, 52] showed that the combination of low mean hydrophobicity and relatively high net charge represents a prerequisite for the absence of compact structure in proteins under physiological conditions. In particular, it was shown that the charge-hydrophobicity phase-space can be divided into two regions by the empirical separatrix line of equation:

$$\langle H \rangle_{boundary} = \frac{\langle R \rangle + 1.151}{2.785} \quad (5)$$

where  $H$  refers to hydrophobicity and  $R$  to the charge. The proteins located below this line in the phase-space are likely to be unfolded in physiologic conditions whereas those lying above the separatrix do fold in a compact, globular conformation. In order to test this issue, the mean hydrophobicity and the mean net charge were computed for the CD loop, for the portion of the protein

Molecular Region	$\langle R \rangle$	$\langle H \rangle$	$\langle H \rangle_{Bound}$
Full Protein	0.546	0.417	0.609
CD Loop	0.507	0.343	0.595
Outside CD Loop	0.563	0.450	0.615

TABLE II: Positions in the charge-hydrophobicity phase-space of three molecular regions of Domain C5 of MyBP-C. The CD loop, the full C5 domain and the portion of the protein excluding the CD loop all lie in the natively unfolded region of the phase-space below the separatrix (Eq 5).

sequence not including this loop and for the whole protein sequence. Following Uversky, in these calculations the hydrophobicity of individual residues was normalized to a scale of 0 to 1, and the mean hydrophobicity is computed as the sum of the normalized hydrophobicities divided by the number of residues in the protein segment under examination. A similar approach was used for the computation of the mean charge. Table II shows that the CD loop is located in the natively unfolded region of the phase space. The full sequence of the C5 domain is closer to the boundary of the natively folded region that, however, it cannot reach due to the effect of the CD loop in the computation of the average charge and hydrophobicity. Finally the portion of the polypeptide sequence not including the CD loop is even closer to the boundary but it still relies in the natively unfolded region due to the features of the minor loops. The properties of the CD sequence were further studied by analyzing the average number of native contacts per amino-acid as suggested in Ref. [53]. According to this approach, natively unfolded proteins are supposed to form a number of native interactions insufficient to compensate for the loss of conformational entropy, hence their necessity to couple folding with specific ligand binding. As a consequence, natively unfolded proteins are expected to feature an average number of contacts lower than that of globular proteins.

Natively unfolded and globular proteins can also be discriminated through a set of 20 artificial parameters designed through Monte Carlo maximization [53] of the scoring function  $Score = (\langle X_f \rangle - \langle X_u \rangle) / \sqrt{S_f^2 + S_u^2}$  where  $\langle X_f \rangle$  and  $\langle X_u \rangle$  are the mean values of the adjustable parameters in two training dataset of folded and natively unfolded proteins and  $S_f$  and  $S_u$  are the corresponding standard deviations.

We generated the profiles of the average number of contacts per residue and of the artificial parameters by shifting a 5-residue window along the protein sequence and assigning the window average to the central residue, so that data in Fig. 9 can be compared to the charge and hydrophobicity plots of Fig. 8, determined with the same procedure. The profiles of the average number of contacts and of the artificial parameters in Figure 9, show that both indicators are effective in discriminating  $\beta$ -strands and unstructured loops, the latter being characterized

by much lower values of the parameters. These results

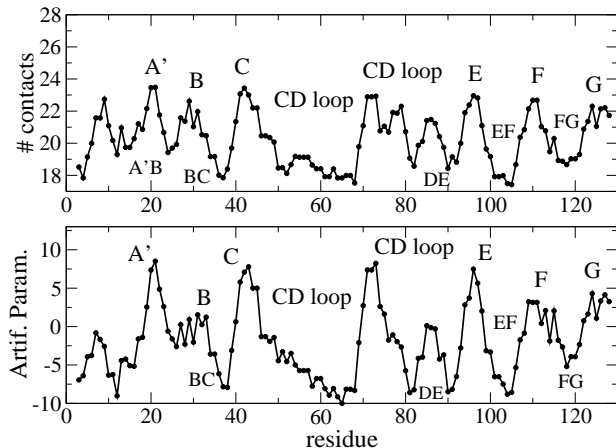


FIG. 9: Profiles of average number of contacts (top) and artificial parameters (bottom) along the sequence of C5 domain. The computation was performed using the parameters listed in Table I of Ref. [53]. The loops are characterized by lower values of both indicators with respect to the strand subsequences.

thus suggest that the CD loop of domain C5 of MyBP-C should be classified as a *natively unfolded sequence* *i.e.* it is protein fragment that lacks a stable structure even in physiological conditions. A common feature of natively unfolded proteins is that their folding is usually associated with the binding to a specific ligand. It could thus be suggested that the long CD loop that appears structureless when the C5 domain is dissected from MyBP-C, might actually be well folded *in vivo* due to a close interaction with a specific ligand. This hypothesis is further supported by the experimental finding that cardiac MyBP-C co-purifies with the Calmodulin class-II (CaM-II)-like Kinase [18, 54, 55] so that the folding of the CD loop may be accompanied by docking with this enzyme.

#### IV. DISCUSSION AND CONCLUSIONS

The involvement of MyBP-C in Familial Hypertrophic Cardiomyopathy motivated a study of the folding of domain C5 through equilibrium MD simulations to gain insight into the role of the three FHC-related mutations: Asn115Lys, Arg14His and Arg28His. As a member of the Immunoglobulin family, domain C5 lends itself to be reasonably modeled through a G $\bar{o}$ -like force field [21]. We assessed the thermodynamics impact of a mutation through the entity of the shift in the folding temperature. Our results show that, among the three FHC-related mutations we examined, Asn115Lys determines the largest decrease in  $T_f$ , in agreement with the NMR spectra recorded by Idowu [16] signalling absence of structure even at low temperature. Conversely, the  $T_f$  shift induced by the Arg28His mutation is modest, while the protein desta-

bilization induced by Arg14His is negligible as its thermogram is almost perfectly superposable to that of the WT. This finding suggests that the latter two mutants have very little effect on protein stability and their pathological role must be sought elsewhere. Both mutations Arg14His and Arg28His imply the removal of three contacts and their impact in the G $\bar{o}$ -like approach could be partially resolved only through the introduction of heterogeneous energetic couplings suggesting the opportunity of a more refined analysis.

Further insights in the role of Arg14 located in the N-terminus of the C5 domain, were attained through the study of the  $\Delta 1 - 7$  deletion mutant. The significant decrease in  $T_f$  of the truncated domain indicates that the N-terminal region with its 10-residue long insert typical of the cardiac isoform, is not just a linker between the C4 and C5 domains, but it gives an important contribution to the stability. However, the low betweenness of the N-terminal residues indicates that they may be involved in contacts forming a subgraph only weakly connected to the core of the contact network. It is thus possible that the N-terminal contacts do appear only when the C5 domain is dissected from the rest of the protein and that the natural role of this section is more related to the binding with domain C8 complementing the negatively charged CFGA' surface [16].

This potential role of the FHC-related mutations is confirmed by the analysis of  $\Phi$ -values that appear to be significantly higher in the CFGA' sheet where Asn115 is located, than in the BDE sheet that including Arg268.

A final issue considered in the present work, is a analysis of the CD loop responsible for the low stability of the C5 domain as compared with other Ig domains. The charge unbalance and the low hydrophobicity of the CD loop, accompanied by a low average number of native contacts and a low value of the artificial parameters introduced by Galzitskaya [53], is a clear indication that the C5 domain of MyBP-C can be considered a *natively unfolded* protein *i.e.* a protein that lacks a compact, globular structure under physiological conditions [48, 49, 50, 51, 52]. Therefore the role of the CD loop of the C5 domain of the cardiac isoform of MyBP-C, must be reconsidered within the framework of the peculiar properties of natively unfolded proteins. As the cardiac MyBP-C co-purifies with the Calmodulin class-II (CaM-II) like Kinase, the CD loop may represent an SH3 domain recognition region [18, 54, 55]. In experiments and simulations performed on the C5 domain alone, the CD loop due to its high mobility, destabilizes the protein, lowering its folding temperature. *In vivo*, however, the CD loop may fold upon binding with the CaM-II-like Kinase, so that the thermodynamic stability and the folding temperature of the protein may be similar to those of the other Ig domains. Our results also suggest that the cardiac C5 domain might regulate the activity of the CaM-II-like Kinase whose docking may trigger the folding of the CD loop. In such a case, the C5 domain may be not only a structural component of the Moolman-Smook



collar (Fig. 1) but it also may play an important role in

the regulation of muscular contraction.

- 
- [1] Winegrad, S. Myosin binding protein c, a potential regulator of cardiac contractility. *Circ. Res.* 2000; 86:6–7.
- [2] Chung MW., Tsoutsman T., Semsarian C. Hypertrophic cardiomyopathy: from gene defect to clinical disease. *Cell. Res.* 2003; 13:9–20.
- [3] Kimura A., Harada H., et al. Mutations in the cardiac troponin i gene associated with hypertrophic cardiomyopathy. *Nat. Genet.* 1997; 16:379–382.
- [4] Mogensen J., Klausen IC., et al.  $\alpha$ -cardiac actin is a novel disease gene in familial hypertrophic cardiomyopathy. *J. Clin. Invest.* 1999;103:R39–43.
- [5] Poetter K., Jiang H. et al. Mutations in either the essential or regulatory light chains of myosin are associated with a rare myopathy in human heart and skeletal muscle. *Nat. Genet.* 1996;13:63–69.
- [6] Satoh M., Takahashi M. et al. Structural analysis of the titin gene in hypertrophic cardiomyopathy: identification of a novel disease gene. *Biochem. Biophys. Res. Commun.* 1999;262:411–417.
- [7] Niimura H. Mutations in the gene for cardiac myosin-binding protein c and late-onset familial hypertrophic cardiomyopathy. *N. Engl. J. Med.* 1998;338:1248–1257.
- [8] Richard P., Charron P. Hypertrophic cardiomyopathy: Distribution of disease genes, spectrum of mutations, and implications for a molecular diagnosis strategy. *Circulation* 2003;107:2227–2232.
- [9] Charron P., Dubourg O., Desnos M. et al. Genotype-phenotype correlations in familial hypertrophic cardiomyopathy. a comparison between mutations in the cardiac protein-c and the  $\beta$ -myosin heavy chain genes. *Eur. Heart J.* 1998;19:139–45.
- [10] Daehmlow S., Erdmann J., Knueppel T. et al. Novel mutations in sarcomeric protein genes in dilated cardiomyopathy. *Biophys. Res. Commun.* 2002;298:116–20.
- [11] Yu B., French JA., Carrier L. et al. Molecular pathology of familial hypertrophic cardiomyopathy caused by mutations in the cardiac myosin binding protein c gene. *J. Med. Genet.* 1998;35:205–10.
- [12] Moolman-Smook J., Flashman E., de Lange W., Li ZL., Corfield V., Redwood C., and Watkins H. Identification of novel interactions between domains of myosin binding protein-c that are modulated by hypertrophic cardiomyopathy missense mutations. *Circ. Res.* 2002;91:704–711.
- [13] Flashman E., Redwood C., Moolman-Smook J., Watkins H. Cardiac myosin binding protein c: Its role in physiology and disease. *Circ. Res.* 2004;94:1279–1289.
- [14] Kunst G., Kress KR., Gruen M., Uttenweiler D., Gautel M., Fink RHA. Myosin binding protein c, a phosphorylation-dependent force regulator in muscle that controls the attachment of myosin heads by its interaction with myosin s2. *Circ. Res.* 2000;86:51–58.
- [15] Redwood CS., Moolman-Smook JC., Watkins H. Properties of mutant contractile proteins that cause hypertrophic cardiomyopathy. *Cardiovasc. Res.* 1999;44:20–36.
- [16] Idowu SM., Gautel M., Perkins SJ., Pfuhl M. Structure, stability and dynamics of the central domain of cardiac myosin binding protein c (mybp-c): Implications for multidomain assembly and causes for cardiomyopathy. *J. Mol. Biol.* 2003;329:745–761.
- [17] Oakley CE., Hambly BD., Curmi PMG., Brown, LJ. Myosin binding protein c: Structural abnormalities in familial hypertrophic cardiomyopathy. *Cell Res.* 2004;14:95–110.
- [18] Hartzell HC., Glass, DB. Phosphorylation of purified cardiac muscle c-protein by purified camp-dependent and endogenous  $\text{Ca}^{2+}$ -calmodulin-dependent protein kinases. *J. Biol. Chem.* 1984;259:15587–96.
- [19] Singh L., Oakley C., Brown LJ., Hambly B. Structural effects of hypertrophic cardiomyopathy mutations on sarcomeric proteins. *Biophys. J.* 2003;84:452.
- [20] Morner S., Richard P., Kazzam E., et al. Identification of the genotypes causing hypertrophic cardiomyopathy in northern sweden. *J. Mol. Cell. Cardiol.* 2003;35:841–9.
- [21] Clarke J., Cota E., Fowler SB., Hamill S. Folding studies of immunoglobulin-like  $\beta$ -sandwich proteins suggest that they share a common folding pathway. *Structure* 1999;7:1145–1153.
- [22] Matysiak S., Clementi C. Optimal combination of theory and experiment for the characterization of the protein folding landscape of S6: how far can a minimalist model go ? *J. Mol. Biol.* 2004;343:235–248.
- [23] Riddle DS., Grantcharova VP., Santiago JV., Alm E., Ruczinski I., Baker D. Experiment and theory highlight role of native state topology in sh3 folding. *Nature Struct. Biol.* 1999;6:1016–1024.
- [24] Chiti F., Taddei N., White PM., Bucciantini M., Magherini F., Stefani M., Dobson, CM. Mutational analysis of acylphosphatase suggests the importance of topology and contact order in protein folding. *Nature Struct. Biol.* 1999;6:1005–1009.
- [25] Plaxco KW., Simons KT., Baker D. Contact order, transition state placement and the refolding rates of single domain proteins. *J. Mol. Biol.* 1998;277:985–994.
- [26] Cecconi F., Micheletti C., Carloni P., Maritan A. The structural basis of antiviral drug resistance and role of folding pathways in hiv-1 protease. *Proteins Struct. Funct. Genet.* 2001;43:365–372.
- [27] Micheletti C., Cecconi F., Flammini A., Maritan A. Crucial stages of protein folding through a solvable model: Predicting target sites for enzyme-inhibiting drugs. *Protein Sci.* 2002;11:1878–1887.
- [28] Hoang TX., Cieplak M. Sequencing of folding events in Go-type proteins. *J. Chem. Phys.* 2000;113:8319–8328.
- [29] Cecconi F., Guardiani C., Livi R. Testing simplified protein models of the hpin1 ww domain. *Biophys. J.* 2006;91:694–704.
- [30] Kouza M., Chang CF., Hayryan S., Yu T., Li MS., Huang TH., Hu CK. Folding of the protein domain hbSBD . *Biophys. J.* 2005;89:3353–3361.
- [31] Stoycheva AD., Brooks III CL., Onuchic JN. Gatekeepers in the ribosomal protein S6: thermodynamics, kinetics, and folding pathways revealed by a minimalist protein model. *J. Mol. Biol.* 2004;340:571–585.
- [32] Clementi C., Nymeyer H., Onuchic JN. Topological and energetic factors: what determines the structural details of the transition state ensemble and "en-route" interme-

- diates for protein folding ? *J. Mol. Biol.* 2000;298:937–953.
- [33] Evans DJ., Hoover WG., Failor BH., Moran B., Ladd AJC. Non-equilibrium molecular dynamics via gauss's principle of least constraint. *Phys. Rev. A.* 1983;28:1016–1021.
- [34] Miyazawa S., Jernigan RL. Estimation of effective interresidue contact energies from protein crystal structures: quasi-chemical approximation. *Macromolecules* 1985;18:534–552.
- [35] Karanicolas J., Brooks III CL. The origins of asymmetry in the folding transition states of protein L and protein G. *Protein Sci.* 2002;11:2351–2361.
- [36] Serrano L., Kellis J., Cann P., Matouschek A., Fersht A. The folding of an enzyme. II. Substructure of barnase and the contribution of different interactions to protein stability. *J. Mol. Biol.* 1992;224:783–804.
- [37] Kurochkina N., Lee B. Hydrophobic potential by pairwise surface area sum. *Protein Engineering* 1995;8:437–442.
- [38] Richards FM., Lee B. The interpretation of protein structures: Estimation of static accessibility. *J. Mol. Biol.* 1971;55:379–400.
- [39] Sung S. Monte-Carlo simulations of  $\beta$ -hairpin folding at constant temperature. *Biophys. J.* 1999;76:164–175.
- [40] Zhou H., Zhou Y. Quantifying the effect of burial of amino acid residues on protein stability. *Proteins Struct. Func. Bioinf.* 2004;54:315–322.
- [41] Vendruscolo M., Dokholyan NV., Paci E., Karplus M. Small-world view of the amino acids that play a key role in protein folding. *Phys. rev. E* 2002;65:61910–61913.
- [42] Dijkstra EW. A note on two problems in connexion with graphs *Numer. Math.* 1959;1:269-271.
- [43] Kaya H., Chan HS. Polymer principles of protein calorimetric two-state cooperativity. *Proteins Struct. Func. Genet.* 2000;40:637-661.
- [44] Zhou Y., Hall CK., Karplus M. The calorimetric criterion for a two-state process revisited. *Protein Sci.* 1999;8:1064-1074.
- [45] Hamill SJ., Steward A., Clarke J. The folding of an immunoglobulin-like greek key protein is defined by a common-core nucleus and regions constrained by topology. *J. Mol. Biol.* 2000;297:165–178.
- [46] Kabsch W. Solution for best rotation to relate two sets of vectors. *Acta Crystallogr.* , 1976;32:922–923.
- [47] Kyte J., Doolittle RF. A simple method for displaying the hydrophobic character of a protein. *J. Mol. Biol.* 1982;157:105–132.
- [48] Dunker AK., Garner F., Guillot S., Romero P., Albrecht K., Hart J., Obradovic Z., Kissinger C., Villafranca JE. Protein disorder and the evolution of molecular recognition: theory, predictions and observations. *Pac. Symp. Biocomput.* 1998;3:473–484.
- [49] Garner E., Cannon P., Romero P., Obradovic Z., Dunker AK. Predicting disordered regions from amino acid sequence: common themes despite differing structural characterization. *Genome Inform.* 1998;9:201–214.
- [50] Romero P., Obradovic Z., Kissinger CR., Villafranca JE., Garner E., Guillot S., Dunker, AK. Thousands of proteins likely to have long disordered regions. *Pac. Symp. Biocomput.* 1998;3:437–448.
- [51] Uversky VN., Gillespie JR., Fink AL. Why are "natively unfolded" proteins unstructured under physiologic conditions ? *Protein Struct. Funct. Genet.* 2000;41:415–427.
- [52] Uversky VN. Natively unfolded proteins: a point where biology waits for physics. *Protein Sci.* 2002;11:739–756.
- [53] Garbuzynskiy SO., Lobanov MY., Galzitskaya OV. To be folded or to be unfolded ? *Protein Sci.* 2004;13:2871–2877.
- [54] Redwood CS., Moolman-Smook JC., and Watkins H. Properties of mutant contractile proteins that cause hypertrophic cardiomyopathy. *Cardiovasc. res.* 1999;44:20–36.
- [55] Gautel M., Zuffardi O., Freiburg A., Labeit S. Phosphorylation switches specific for the cardiac isoform of myosin binding protein-c: a modulator of cardiac contraction? *EMBO J.* 1995;14:1952–60.